

## Materials and Methods

### Animal husbandry

*Schmidtea mediterranea* clonal asexual strain CIW4 animals, starved for 7–14 days prior experimentation, were used for all experiments except for *in situ* hybridizations in embryos (Fig. 1). All animals utilized were healthy, not previously used in other procedures, and were of wild-type genotype. Animals were cultured in plastic containers or petri dishes for experiments, in 1x Montjuic water (1.6 mmol/l NaCl, 1.0 mmol/l CaCl<sub>2</sub>, 1.0 mmol/l MgSO<sub>4</sub>, 0.1 mmol/l MgCl<sub>2</sub>, 0.1 mmol/l KCl and 1.2 mmol/l NaHCO<sub>3</sub> prepared in Milli-Q water) at 20°C in the dark. Animals were fed blended calf liver. *Schmidtea polychroa* lines were generated by amputation of a starter animal and the line was initially propagated through successive rounds of amputation. After generating a large colony, lines were propagated through sexual reproduction. Animals were fed homogenized beef liver once a week and cleaned twice weekly. Animals were kept in the dark at 20°C and maintained in 1x Montjuic water. Egg capsules were collected and staged daily (68).

### Replication, size estimation and randomization

At least two independent FISH and immunostaining experiments with a minimum of three animals/experiment were performed for the characterization of muscle guidepost cells in intact and regenerating adults and in embryos. For RNAi phenotype characterization, numbers of animals used in each staining are indicated in each panel. No sample size estimation was performed. Animals for all experiments were randomly selected from a large collection of clonal animals. All animals have been included in statistical analyses, no exclusions have been done. Images were randomized before quantification.

### Gene nomenclature

Genes that encode proteins with a clear domain structure have been assigned a name accordingly but also identified using a transcriptome contig id number to facilitate identification (figs. S7 and S8).

### Drop-seq clustering and single-cell differential expression analysis

To obtain transcriptomes for NMEs and NMCs, data from targeted single-cell sequencing of the planarian brain ((62), GEO accession number GSE111764, BrainClusteringDigitalExpressionMatrix.dge.txt.gz) was used to identify cells positive for expression of *notum* (dd\_Smed\_v4\_24180\_0\_1) and *fz5/8-4* (dd\_Smed\_v4\_11823\_0\_1) and negative for expression of the anterior pole marker *foxD* (dd\_Smed\_v4\_23249\_0\_1) and the neuronal markers *ChAT* (dd\_Smed\_v4\_6208\_0\_1) and *pc2* (dd\_Smed\_v4\_1566\_0\_1) (log-scale expression of 0.5 for all genes). To identify these cells within the single-cell sequencing data, the Seurat function WhichCells [subset.name=contig ID, accept.low=0.5] was used with Seurat package, v2.2 (69). Fifteen cells satisfied all gene expression thresholds (Cells\_Head1\_AAGTCTCAGGCC, Cells\_Head1\_CAGACCTTCCCC, Cells\_Head1\_CGTGACTAAGAA, Cells\_Head1\_GGCGTGGTGACN, Cells\_Head1\_TAAATTCGATAG, Cells\_Head1\_TTTACTTTTCGAT, Cells\_Head2\_AACGCCATTTCC, Cells\_Head2\_AGTATGAATATG, Cells\_Head2\_AGTCACTAACAA, Cells\_Head2\_CACCGTGTACTA, Cells\_Head2\_CCAGATAACGCA, Cells\_Head2\_CGTAACTATCGT, Cells\_Head2\_GGTTACAGCTTT, Cells\_Head2\_GTTCCATGAAGN, Cells\_Head2\_TGCTGTGCATCT). Of these fifteen cells, eight cells were assigned a muscle identity in (62) (Cells\_Head2\_AACGCCATTTCC, Cells\_Head2\_AGTATGAATATG, Cells\_Head2\_AGTCACTAACAA, Cells\_Head2\_CACCGTGTACTA, Cells\_Head2\_CCAGATAACGCA, Cells\_Head2\_CGTAACTATCGT, Cells\_Head2\_GGTTACAGCTTT, Cells\_Head2\_TGCTGTGCATCT). Additional data on identified cells can be found in Table S1 of (62). An expression matrix for all cells identified as muscle in the targeted

brain sequencing from (62) was generated, tagging the eight muscle cells above as positive and the remaining 522 muscle cells as negative. This expression matrix was used as input for the R package SCDE (70). SCDE analysis revealed a list of genes enriched in these putative guidepost cells. Genes were ranked by their 'conservative expression' value. To obtain transcriptomes for *notum*<sup>+</sup> brain neurons, cells identified as neural from the targeted brain sequencing were combined with all cells identified as neural in the principal single-cell sequencing from (62). Cells positive for expression of both *ChAT* (log-scale expression of 2.5) and *notum* (log-scale expression of 2) were identified, as above. Thirteen cells satisfied both gene expression thresholds (Cells\_Head\_TCATCCACGCTT, Cells\_Head\_ACAATGTTTGGT, Cells\_Head\_GTCAGACTCAGN, Cells\_Head\_CCTGTCGGCTCN, Cells\_Head\_AGGGCGTAGTAA, Cells\_Head2\_GTCGTCGTTGCG, Cells\_Head2\_GGCCCGAGGATG, Cells\_Whole\_CGAACCAATAGT, Cells\_Pharynx\_AGTACAATGTGN, Cells\_Head2\_AAACCAAGCCAG, Cells\_Head2\_AGTTAGGCACAN, Cells\_Pharynx\_GGTAGGTTATCG, Cells\_Pharynx\_AAGTAGGCATCG). Of these thirteen cells, three had been isolated from the planarian pharynx (Cells\_Pharynx\_AGTACAATGTGN, Cells\_Pharynx\_GGTAGGTTATCG, Cells\_Pharynx\_AAGTAGGCATCG) and were thus discarded. Additional data on identified cells can be found in Table S1 of (62). An expression matrix for all *ChAT*<sup>+</sup> neurons (2103 cells) was generated, tagging the name of each neuron as positive or negative for expression of *notum*. This expression matrix was used as input for analysis by SCDE, as above, revealing a list of genes enriched in *notum*<sup>+</sup> neurons. Genes were ranked by their 'conservative expression' value.

For all cells analyzed in Table S1, UMI counts were log normalized by dividing by the total number of UMIs per cell, then multiplying by 10,000. All calculations were performed in log space (i.e.  $\ln(\text{UMIs-per-}10,000+1)$ ). The fifty transcripts with the highest average normalized expression in the 8 putative guidepost-like cells were then identified and their expression was compared with 10 randomly chosen non-guidepost muscle cells (chosen from cluster 9 of the Drop-seq data), 10 randomly chosen ciliated epidermis cells (chosen from cluster 19 of the Drop-seq data), and 10 randomly chosen neural cells (chosen from clusters 0,1,5,17,20,23,24,25,26,27, and 28 of the Drop-seq

data). Averages indicate the average normalized UMI counts for each group of cells. Muscle enrichment/broad expression determinations were made using the online resource [digiworm.wi.mit.edu](http://digiworm.wi.mit.edu) from (62). Namely, genes enriched in clusters 7, 13, 14, or 16 of the main clustering data from (62), but not broadly expressed across most clusters, were designated muscle enriched. All of the top 50 transcripts expressed in the putative guidepost cells were either muscle enriched or broadly expressed, including in muscle.

### Gene cloning

Homologs of guidance cues in planarians were cloned using the following primers:

*roboC* (dd\_Smed\_v4\_7921\_0\_1), fwd: 5' atggtgccattgtcccg; rv: 5' aaccgagagttgccggtg;

*roboD* (dd\_Smed\_v4\_14150\_0\_1), fwd: 5' tgctcaatcgtcagataccg; rv: 5' accgggaattcgaaaagact

*unc-5A* (dd\_Smed\_v4\_10380\_0\_1), fwd: 5' ttgctcctagcgggtctcat; rv: 5' tgtacgcggaattgctactg

*unc-5B* (dd\_Smed\_v4\_10585\_0\_1), fwd: 5' tcttgagccacaaccctttt; rv: 5' ccagttcgatatccgaagga

*unc-5C* (dd\_Smed\_v4\_10730\_0\_1), fwd: 5' ccaactcgggaaattgaaga; rv: 5' ccgaaacaaaagggtggagaa

*unc-5D* (dd\_Smed\_v4\_16435\_0\_1), fwd: 5' ccctcaaggaacaaaatgga; rv: 5' aaatttccaatcgggtttc

*ephR-1* (dd\_Smed\_v4\_16483\_0\_1), fwd: 5' ccgatcacttttcagccaat; rv: 5' gtgagggttgctgattccat

*ephR-2* (dd\_Smed\_v4\_16928\_0\_1), fwd: 5' gttcctctgatgtgccag; rv: 5' agatccggcatgaatctgac

*ephrin* (dd\_Smed\_v4\_16552\_0\_1), fwd: 5' tccagcaagatatgccgata; rv: 5' tgctgaaaaactgataattgaaaca.

*ephrin* (dd\_Smed\_v4\_10687\_0\_1), fwd: 5'agtcattcacggtccaggc; rv: 5'  
cccatgaaaaacaggttcaaaag

*arrowhead* (dd\_Smed\_v4\_47123\_0\_1), fwd: 5' gttgcaaagctagctcaattca;  
rv: 5' acgggatatggattaacttgaca

*plexin* (dd\_Smed\_v4\_11934\_0\_1), fwd: 5' gcgagtgtggtgggaaaaat; rv: 5'  
ccaagacgcaccaagaacaa

*semaphorin-1* (dd\_Smed\_v4\_12018\_0\_1), fwd: 5'acctgaaatccctttcactcgt;  
rv: 5' tccagctgtgtaagagagga

*soxP-5* (dd\_Smed\_v4\_9050\_0\_1) accession number: GenBank JX010525.1.

All constructs were cloned from cDNA into the pGEM vector (Promega). These constructs were used to synthesize RNA probes and dsRNA for RNAi experiments.

### RNAi

For RNAi experiments, dsRNA was synthesized by *in vitro* transcription reactions (Promega) using PCR-generated templates with flanking T7 promoters, followed by ethanol precipitation, and annealed after resuspension in water. The concentration of dsRNA varied in each prep between 4 and 7 µg/ml. dsRNA was then mixed with planarian food (liver) (36) and 2 µl of this mixture per animal (liver containing dsRNA) was used for feedings. For the guidance cue screen (fig. S8) animals were fed six times in three weeks. For the PCG screen (Fig. 5; fig. S9) animals were fed between six and ten times in three to five weeks until phenotype was observed. *ovo* RNAi animals for homeostasis experiments (Fig. 3, Fig. 5; fig. S9) were fed eight to twelve times during a four to six weeks. *ovo* RNAi regeneration experiments (eye resection and decapitation, Fig. 3) animals were fed eight times in four weeks. *ovo* RNAi animals for transplantation experiments were fed eight times in four weeks (Fig. 4; figs. S5 and S6). *ndk; ndl4* RNAi animals were fed until posterior eyes appeared (8-12 feedings). For RNAi “wear off” experiments, animals were not fed for two months before a midline sagittal cut was performed (Fig. 5). *arrowhead* RNAi animals (Fig. 6; fig. S11) were fed six times over a period of three weeks. *tolloid* RNAi animals for regeneration experiments were fed only

once, and twice for homeostasis experiments (Fig. 6; fig. S10). *soxP-5* RNAi animals were fed eight times in a four-week period of time (Fig. 6; figs. S12 and S13). All feedings were performed every other three days. In all cases, animals were fixed seven days after the last feeding. For regeneration experiments, animals were amputated into three pieces (head, trunk and tail pieces) one week after the last RNAi feeding. Seven days after amputation, trunk pieces were scored, and fixed for further analysis.

### Fluorescence in situ hybridizations and immunostainings

RNA probes were synthesized and whole-mount FISH was performed (36). Briefly, animals were killed in 5% NAC and treated with proteinase K (2 µg/ml). Following overnight hybridizations, samples were washed twice in each of pre-hybridization buffer, 1:1 pre-hybridization-2X SSC, 2X SSC, 0.2X SSC, PBS with Triton-X (PBST). Subsequently, blocking was performed in 10% Western Blocking Reagent (Roche, 11921673001) PBST solution for DIG probes, or in 5% Horse serum and 5% casein for DNP and FITC probes. Antibody washes were then performed for one hour followed by tyramide development. Peroxidase inactivation with 1% sodium azide was done for 90 minutes at room temperature. Brightfield images were taken with a Zeiss Discovery Microscope. Fluorescent images were taken with a Leica SP8 Confocal Microscope. Co-localization analyses of FISH signals were performed using Fiji/ImageJ. 3D reconstruction for the movies was performed using Imaris 3/4D Image Visualization and Analysis Software. For each channel, histograms of fluorescence intensity were used to determine the cut-off between signal and background. All FISH images shown are representative of all images taken in each condition, and are maximal intensity projections. All images, otherwise indicated, are anterior up. For immunostainings with anti-Arrestin antibody (VC-1) or anti-muscle antibody (6G10), animals were fixed as for *in situ* hybridizations, blocked in 3% BSA-PBST or in 10% Western Blocking Reagent (Roche, 11921673001) PBST solution, respectively, for one hour and then stained with the antibody of interest. The anti-muscle mouse monoclonal antibody 6G10 (RRID: AB\_2619613) (71) was used in a 1:1000 dilution, the anti-Arrestin mouse monoclonal antibody VC-1 was used in a 1:5000 dilution, the anti-Arrestin rabbit polyclonal antibody and the anti-alpha tubulin antibody (Lab Vision Cat# MS-581, RRID: AB\_144075) was

used in a 1:500 dilution, and an anti-mouse Alexa conjugated antibodies (Life Tech) were used in a 1:500 dilution. The pool of probes used for labelling muscle cells included *troponin*, *tropomyosin*, *colF-2*, *colF-10* (Fig. 1, fig. S2).

#### *Schmidtea polychroa* (Spol) fluorescence *in situ* hybridization

Whole mount fluorescent *in situ* hybridization was performed as described above for *Schmidtea mediterranea* with the following modifications. 1) Stage 2-5 embryos were dissected out of egg capsules and fixed in 4% formaldehyde for two hours. Embryos were washed in PBSTx-0.5% for 10 minutes and dehydrated in 25%, 50%, 75%, 100% PBSTx:Methanol for 10 minutes. Fixed embryos were not bleached and stored at -20°C. Proteinase K treatment was extended to 20 minutes. 2) Stage 6 and 7 embryos were dissected out of egg capsules and fixed in 4% formaldehyde for one hour. Embryos were washed in PBSTx-0.5% for 10 minutes and dehydrated in 25%, 50%, 75%, 100% PBSTx:Methanol for 10 minutes each. Embryos were washed in PBSTx-0.5% for 10 minutes and dehydrated in 25%, 50%, 75%, 100% PBSTx:Methanol for 10 minutes. Fixed embryos were not bleached and stored at -20°C. Proteinase K treatment was extended to 15 minutes. 3) Hatchlings were treated with 5% NAC PBS with gentle rotation for 5 minutes and then fixed in 4% formaldehyde for one hour. Hatchlings were then washed in PBSTx-0.5% for 10 minutes and dehydrated in 25%, 50%, 75%, 100% PBSTx:Methanol for 10 minutes. Hatchlings were stored at -20°C and bleached in formamide bleaching solution for one hour at room temperature. Proteinase K treatment was extended to 12 minutes. All embryos were mounted in Vectashield between two coverslips and both sides imaged on a Leica SP8 confocal microscope.

#### *Eye resections and eye transplantations*

In order to selectively resect eyes, animals were placed on moist filter paper on a cold block to limit movement, and the tip of a microsurgery blade was used to remove eyes. For eye transplants, after anesthesia using 0.2% Chloretone in planarian H<sub>2</sub>O (1,1,1-Trichloro-2-methyl-2-propanol) for two minutes, a thin slit cut was made to desired locations of the recipient animals and a small hole was generated by gently moving the

surgical blade up and down within the slit cut. Recipient animals were washed in Holtfreter's Solution for 2 minutes and rested in 0.2% Chloretone for 2 minutes, briefly washed in Holtfreter's Solution and transferred on the cold block to introduce the excised eyes. Eye resections were performed using a dissecting microscope by trimming the pigmented tissue around the eyes with a surgical blade, leaving only the white area and the visible optic cup of the eyes. The pigmented ventral side of this tissue was also trimmed away before transplantation. The eyes were gently pushed inside the previously generated holes in the recipient animals. Transplanted animals were immobilized using Type IV, 5% ultra-low melting agarose (Sigma) on top of Whatman™ (GE Healthcare, Life Sciences) filter paper. Solidified gel was covered using Rasta Royale ultrathin rolling paper soaked in Holtfreter's Solution. Transplanted animals were kept in 10°C overnight and recovered by cutting the gel around and also on top of the animal. Animals were placed in planarian H<sub>2</sub>O and kept at 22°C for recovery.

### Quantifications and statistical analysis

Total numbers of NMEs and NMCs were counted based on expression of the markers *notum* and *fz5/8-4*, the location of their nuclei on the dorsal-ventral axis, and using as a reference the brain architecture with a DAPI nuclei staining. Total numbers of muscle guidepost cells were also counted and graph relative to the total length of the animal expressed in  $\mu\text{m}$ .

NME and NMC cell position and density maps were generated by building an idealized planarian visual circuit and positioning it in relation to the brain commissure and the anterior pole determined by DAPI staining and *notum* expression, respectively. This trace was placed on 4 (for *ovo* RNAi only) or 9 (for all other conditions) equal zones in the Adobe Illustrator Software and the approximate positions of NME and NMCs in relation to the photoreceptor axons, brain commissures and anterior poles was mapped manually. Heatmaps indicating relative positions of NME and NMCs were generated by counting the NME and NMCs that fall into each of the 9 zones. The range was



determined by the highest and the lowest total number of cells that were counted in each zone.

Axonal trajectories were manually traced in the Adobe Illustrator Software after transferring a maximum intensity projection of the image containing the planarian visual circuitry into a new document. NME and NMCs were mapped onto the traces based on their position in relation to the visual axons using FIJI's channels tool, determining the dorsal-ventral position for each cell. To determine the significance of axonal interactions with NME, NMC and NBCs (Fig. 2), axons from 6 to 10 separate eyes, for each group, were traced manually in the same manner described above. The trace maps were placed on a circular area that is divided into 36 equal sections (10 degrees each). NME, NMC and NBC cell distributions in reference to the center point of the circle (eye) were mapped and angular median values and 95% confidence intervals for cell positions was calculated for each group. NME/NMC/NBC numbers and the number of axonal intersections in each pie shaped section shown in Fig. 2 were counted and bar graphs were generated using GraphPad Prism software after linearizing the circular arenas. Coincidence of NMEs/NMCs/NBCs and axons was represented by a black box around the area they both occupy (fig. S3). Local axonal trajectories were traced in relation to NME and NMCs in 'd7 after eye transplant' animals and axons that extend within two NME or NMC cell diameters were mapped in circular fields. An overlay map of these circular fields was generated to build a density map of axons that project to the vicinity of NME and NMCs (Fig. 4; fig. S6).

One-way ANOVA test followed by Dunnett's multiple comparison test was used when analyzing more than two conditions. Unpaired Student's *t*-test was used when comparing two conditions. Mean  $\pm$  SD is shown in all graphs.

### **Captions for Tables:**

Table S1. Expression of muscle markers in *notum*<sup>+</sup>; *fz5/8-4*<sup>+</sup> guidepost-like cells.

Table S2. SCDE analysis and list of enriched gene expression in NMEs/NMCs.

Table S3. SCDE analysis and list of enriched gene expression in NBCs.

**Captions for Movies:**

**Movie S1.** Ventral to dorsal view of the visual system showing NMEs and NMCs (*fz5-8/4* (magenta); *notum* (green); anti-Arrestin (yellow)).

**Movie S2.** Three-dimensional reconstruction of the visual system showing NBCs, NMEs and NMCs (*notum* (magenta); anti-Arrestin (cyan); muscle pool (yellow)).

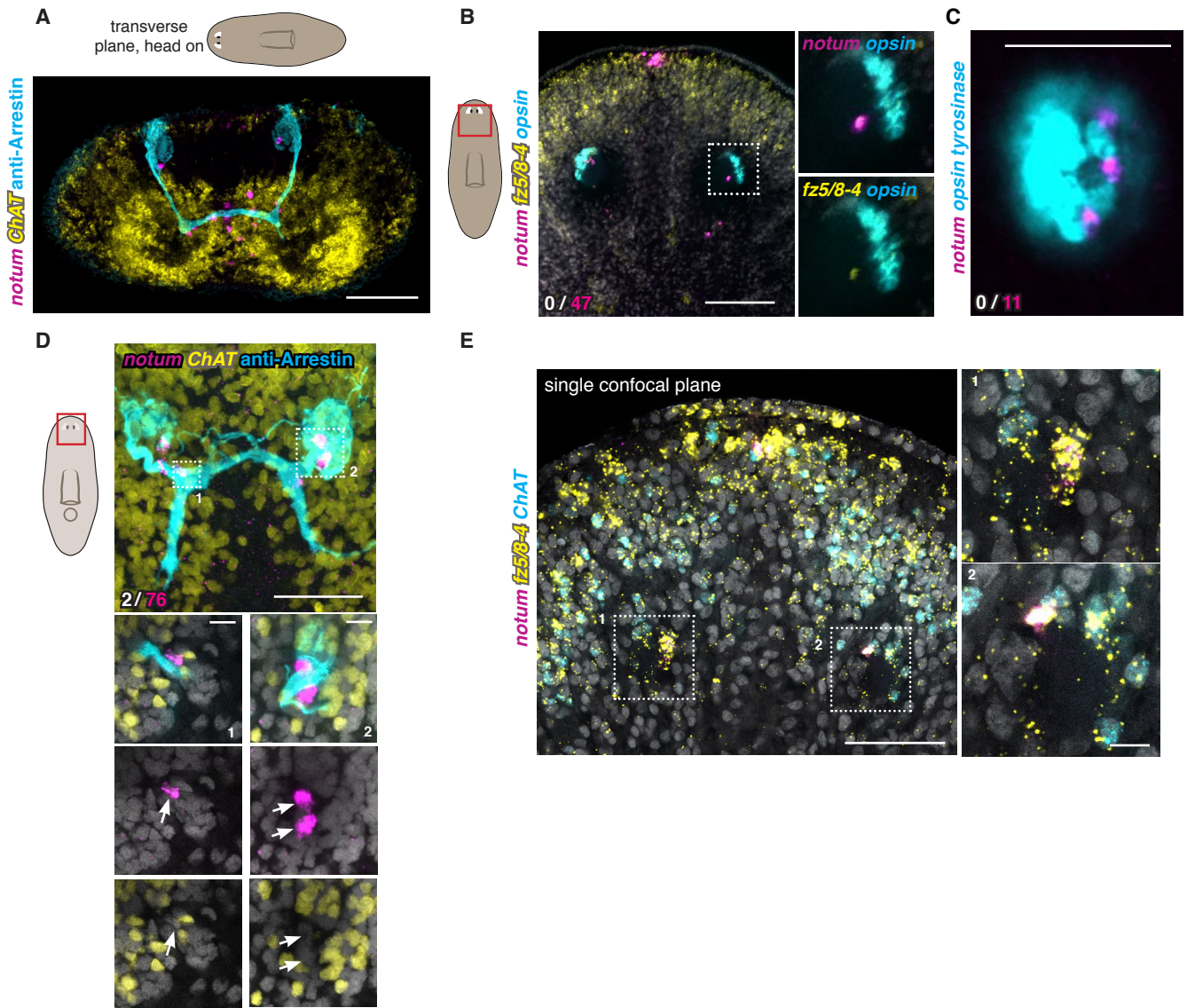


Figure S1

**Figure S1. Characterization of *notum*<sup>+</sup>; *fz5/8-4*<sup>+</sup> cells associated with the visual system.** (A) Dorsoventral view of the visual system showing *notum*<sup>+</sup> cells associated with the visual system and *ChAT*<sup>+</sup> neurons in the brain. (B-D) *notum*<sup>+</sup>; *fz5/8-4*<sup>+</sup> cells associated with visual axons do not express eye-specific markers (B, C), or neuron-specific markers (D). (E) Some *fz5/8-4*<sup>+</sup>; *ChAT*<sup>+</sup> cells that do not express *notum* are observed near *notum*<sup>+</sup>; *fz5/8-4*<sup>+</sup> cells associated with visual axons. Red boxes in cartoons show location of image taken.

Scale bars, 50µm (A-E) and 10µm for all zoom-ins (D, E).

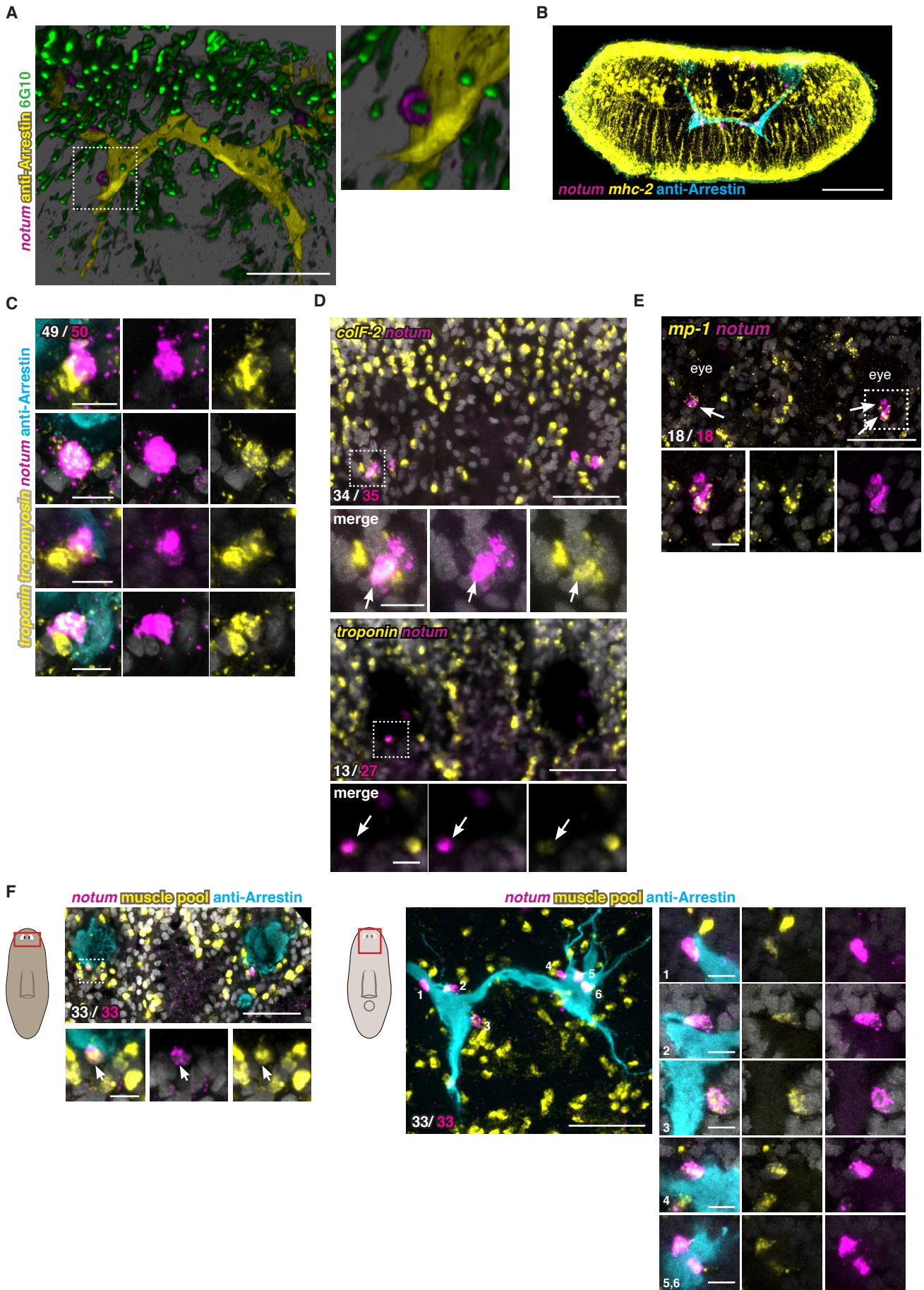


Figure S2

**Figure S2. *notum*<sup>+</sup>; *fz5/8-4*<sup>+</sup> cells associated with the visual system are muscle cells.** (A) A *notum*<sup>+</sup> muscle fiber (labeled with the muscle antibody 6G10) is associated with visual axons. (B) Head on view of dorsoventral muscle fibers (*mhc-2*<sup>+</sup>) shown along with the visual axons and *notum*<sup>+</sup> cells. (C-F) *notum*<sup>+</sup>; *fz5/8-4*<sup>+</sup> cells express muscle-specific markers (F; muscle pool includes *troponin*, *tropomyosin*, *colF-2*, and *colF-10*.) Zoom-ins show co-localization. White arrows show coexpression of *notum*<sup>+</sup> cells associated with the visual system and muscle markers. White dotted boxes show zoom-in areas.

Scale bars, 50µm (A-F) and 10µm for all zoom-ins (C-F).



**Figure S3. Association of NMEs, NMCs, and NBCs with visual axons during regeneration.** (A) Histograms show the distribution of cells (NMCs, light pink top; NMEs, dark pink, middle; and NBCs, orange, bottom) and axons (blue) in different regeneration contexts: eye resection, top; decapitation, middle and bottom. (B) Axonal projections towards NMCs following unilateral eye resection. (C) Axonal projections towards NMEs/NMCs (pink) and NBCs (orange) at different timepoints following head amputation. Dotted pink and orange lines show where NMEs/NMCs and NBCs, respectively, are observed. Dotted white boxes show areas zoom-in below.

Scale bars, 50 $\mu$ m (B, C).



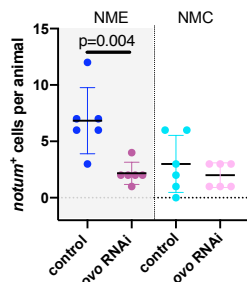
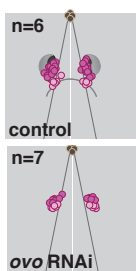
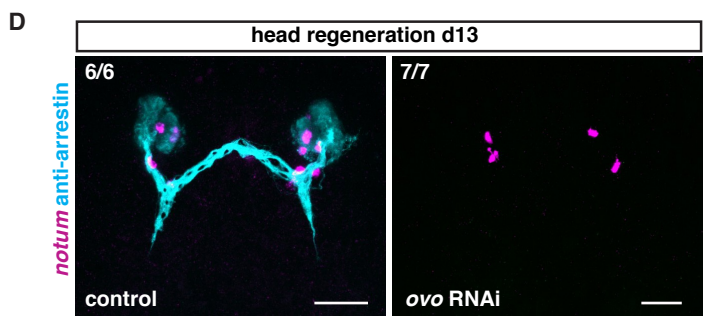
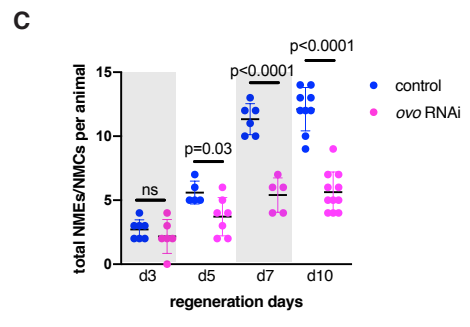
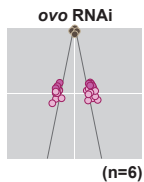
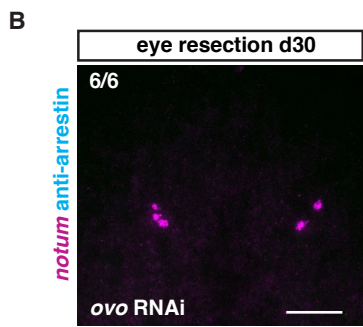
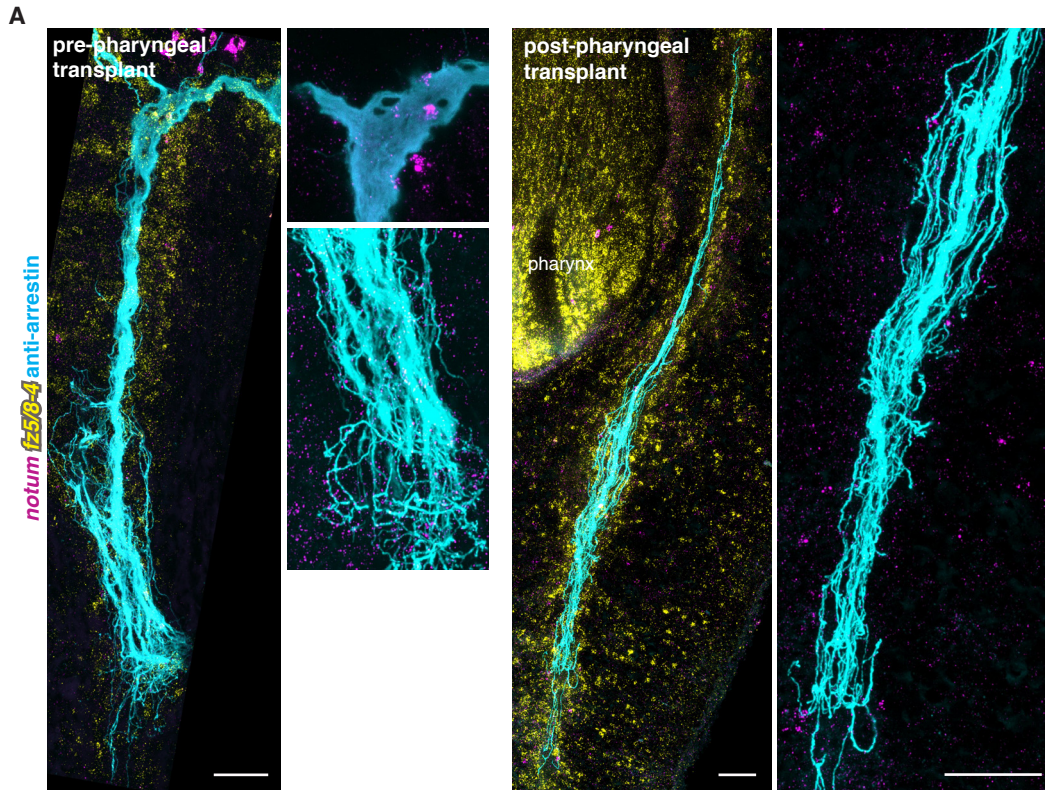


Figure S4

**Figure S4. NMEs and NMCs are specified independently of axons.** (A) NMEs/NMCs are not observed associated with visual axons of transplanted eyes. (B) Presence of NMEs/NMCs in regenerating double-eye resected *ovo* RNAi animals after 30 days. Right: Mapping shows NME/NMC distributions in an idealized visual system cartoon. n indicates number of animals mapped. (C) Graph shows NME/NMC numbers in a regeneration time course in *ovo* RNAi animals. (D) Late regeneration timepoint of an *ovo* RNAi animal showing NMEs/NMCs. Right: Mapping shows NME/NMC distributions in an idealized visual system cartoon. n indicates number of animals mapped. Graph shows NME/NMC numbers.

Scale bars, 50 $\mu$ m (A, B, D).

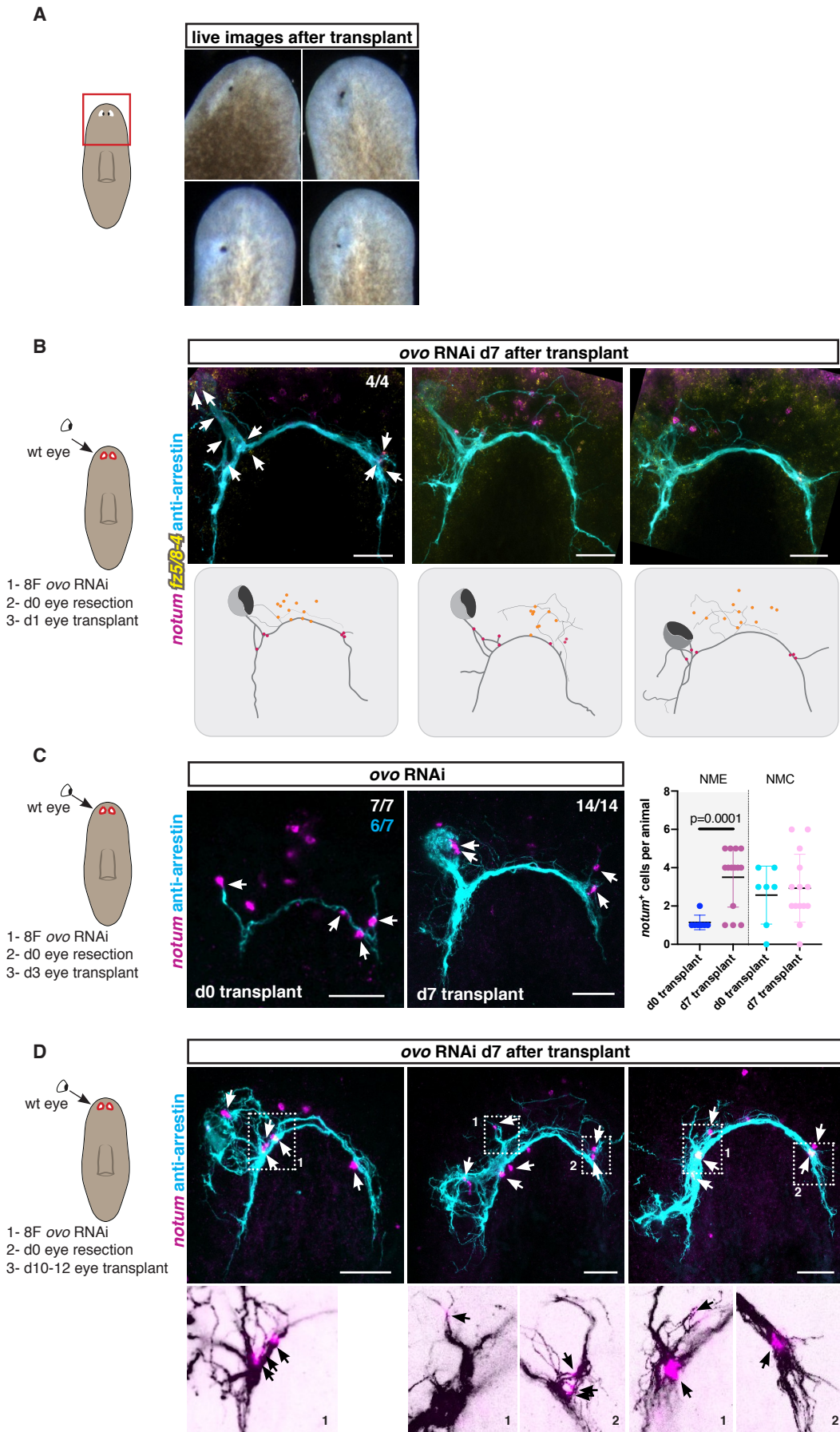


Figure S5

**Figure S5. NMEs and NMCs facilitate visual axons patterning after eye transplantation.** (A) Live images of wildtype eyes transplanted into *ovo* RNAi recipients 7 days after transplantation. (B) Recapitulation of stereotypical visual axonal trajectory in *ovo* RNAi animals transplanted with a wildtype eye one day after double-eye resection. At this time, visual axons from original eyes still remained in the recipient animal. Cartoons show axonal tracings of the image above and position of NMEs, NMCs, and NBCs. (C) Recapitulation of stereotypical visual axonal trajectory in an *ovo* RNAi animal transplanted with a wildtype eye three days after double-eye resection. At this time, 86% of the recipient animals still have visual axons from the original eyes. Right: Graph shows NME/NMC numbers before and after eye transplantation. (D) Recapitulation of stereotypical visual axonal trajectory with more defasciculation in *ovo* RNAi animals transplanted with a wildtype eye 10-12 days after double-eye resection. At this time, only 12.5% of the recipient animals still have visual axons from the original eyes. Below: zoom-ins showing axonal projections of the transplanted eye in close association with NMEs and NMCs (black or white arrows). Cartoons on the left show summarized surgical procedure: animals were RNAi fed 8 times (8F), double-eye resected at day 0, and a single wildtype eye was transplanted one (B), three (C), or 10-12 (A, D) days after resection. Animals were fixed 7 days after transplantation. Pink cells in cartoons are NMEs/NMCs, orange cells are NBCs.

Scale bars, 50 $\mu$ m (B-D).

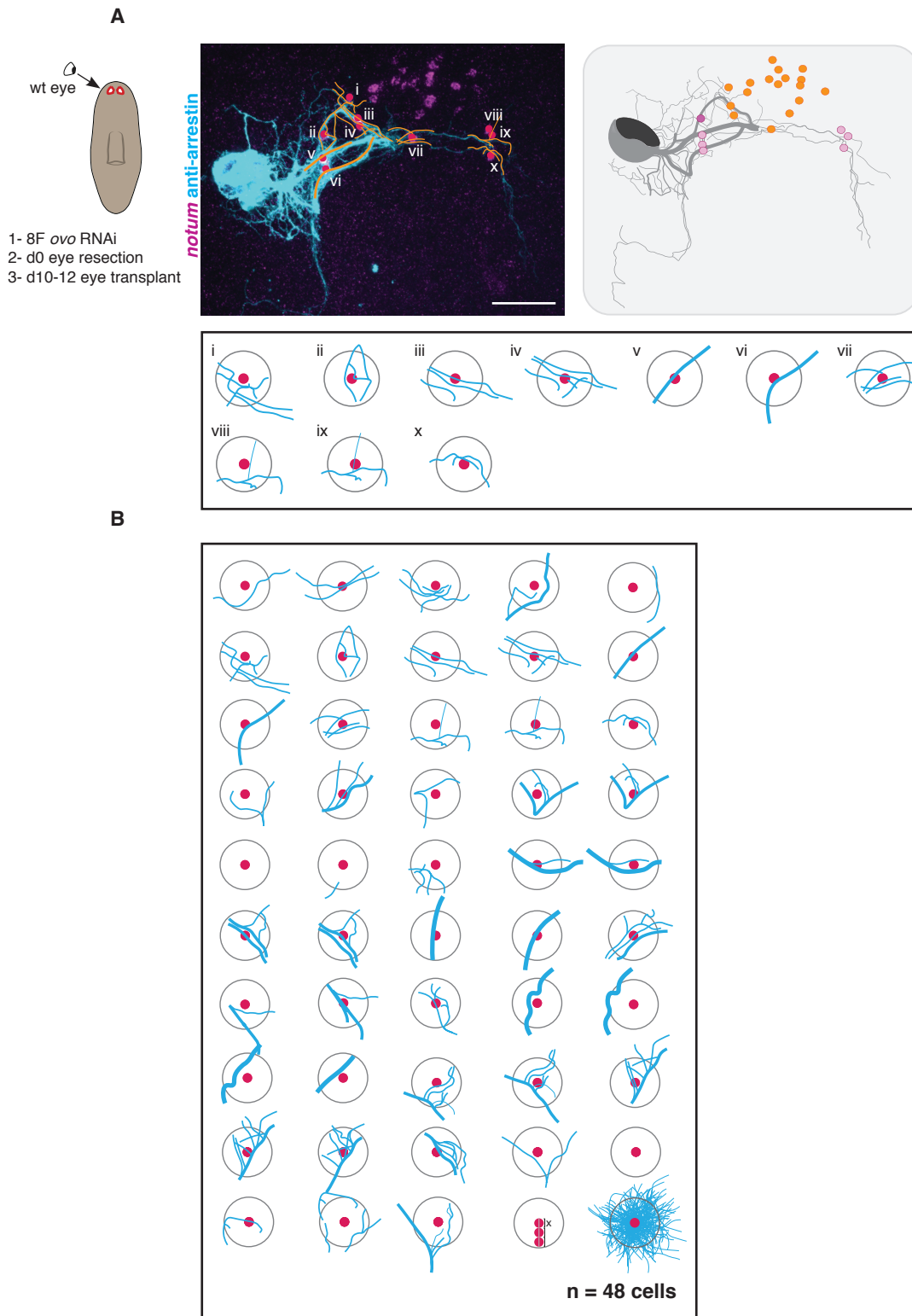


Figure S6

**Figure S6. Visual axonal tracing following eye transplantation.** (A) Example showing how quantification of the association between visual axons and NMEs/NMCs was performed. In orange lines, axonal tracings quantified below in individual circles. Right: Cartoon shows axonal tracings and NME/NMC/NBC distributions of the image shown on the left. Cartoons on the left show summarized surgical procedure: animals were RNAi fed 8 times (8F), double-eye resected at day 0, and a single wildtype eye was transplanted 10-12 days after resection. Animals were fixed 7 days after transplantation. (B) Axonal tracks interacting with individual guidepost-like cells after eye transplantation.

Scale bar, 50 $\mu$ m (A).

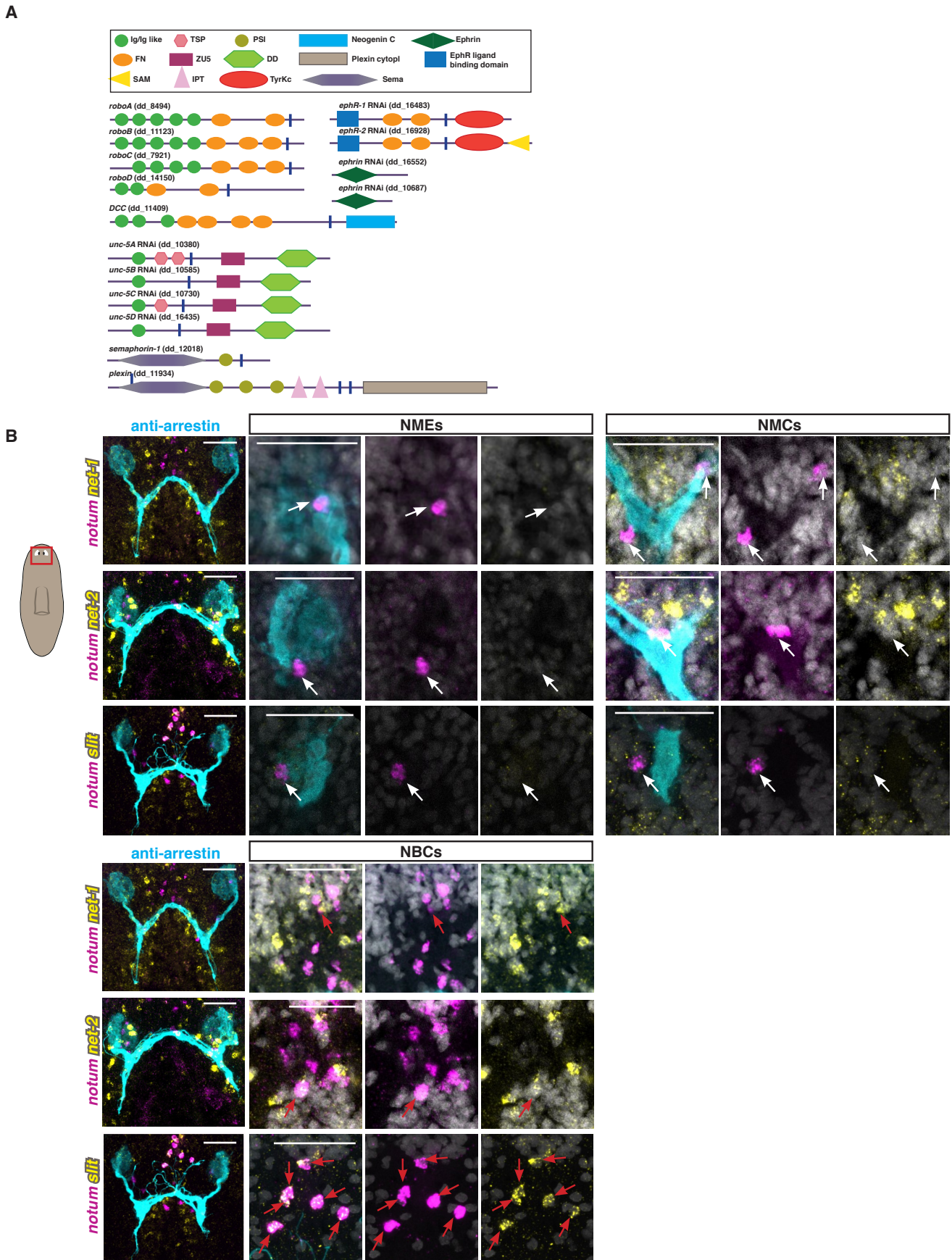


Figure S7

**Figure S7. Identification and coexpression of guidance cues and guidepost-like cells.** (A) Structural domains of canonical guidance cue homolog proteins. (B) Expression of the guidance cues *netrin-1*, *netrin-2*, and *slit* in NMEs, NMCs, and NBCs of intact animals.

Scale bars, 50 $\mu$ m (B).



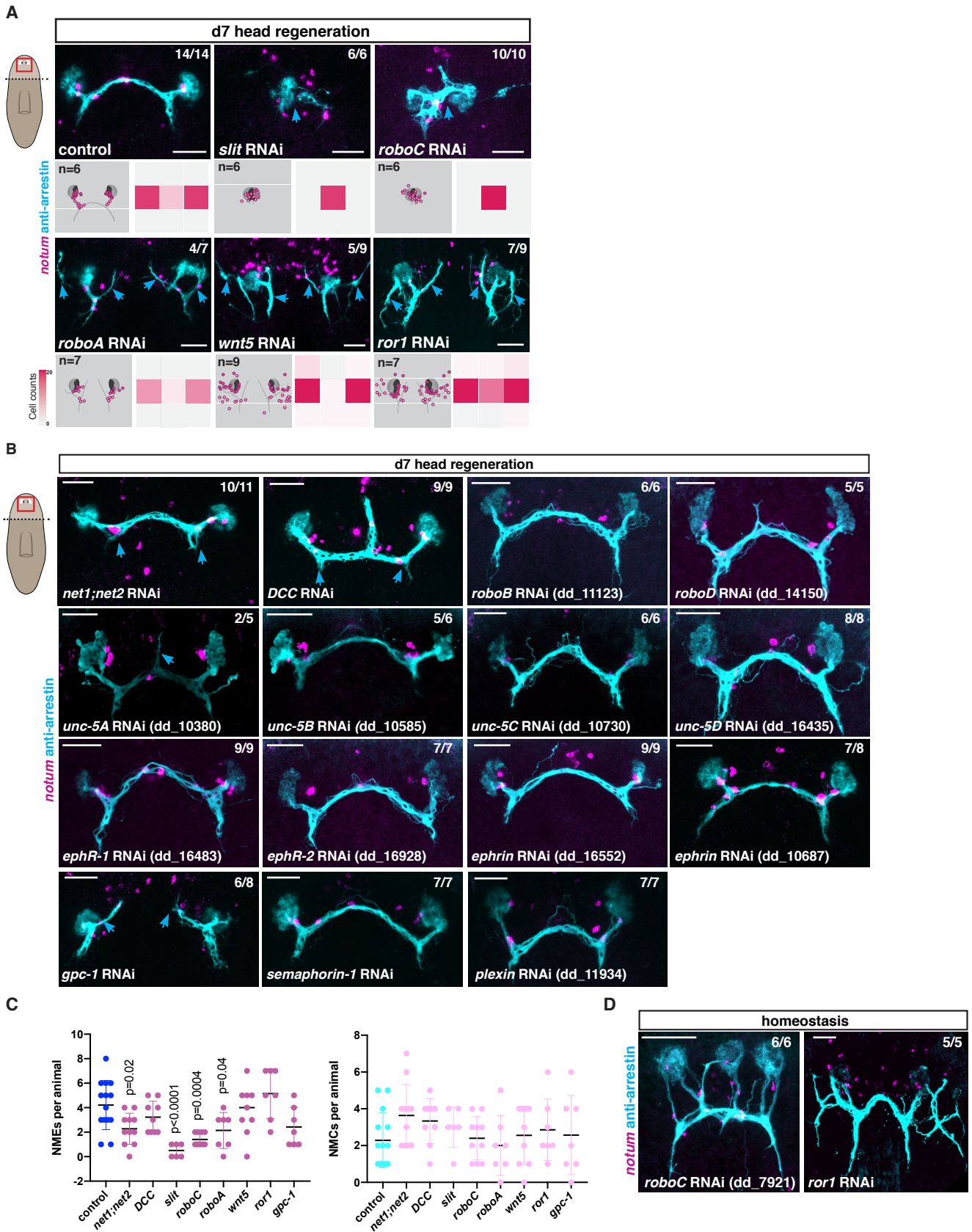


Figure S8

**Figure S8. Role of extrinsic guidance cues and PCGs in the positioning of NMEs and NMCs.**

(A) Top: NMEs/NMCs associated with visual axons 7 days following decapitation in different RNAi conditions. Bottom left: Density map shows NME/NMC distributions in an idealized visual system illustration. n indicates number of animals mapped. Bottom right: Heatmap shows number of NMEs/NMCs located in each quadrant. (B) NMEs/NMCs associated with visual axons 7 days following decapitation in different RNAi conditions. (C) Graph shows NME/NMC numbers in different RNAi conditions. (D) NMEs/NMCs associated with visual axons in uninjured *roboC* and *ror-1* RNAi animals.

Scale bars, 50 $\mu$ m (A, B, D).

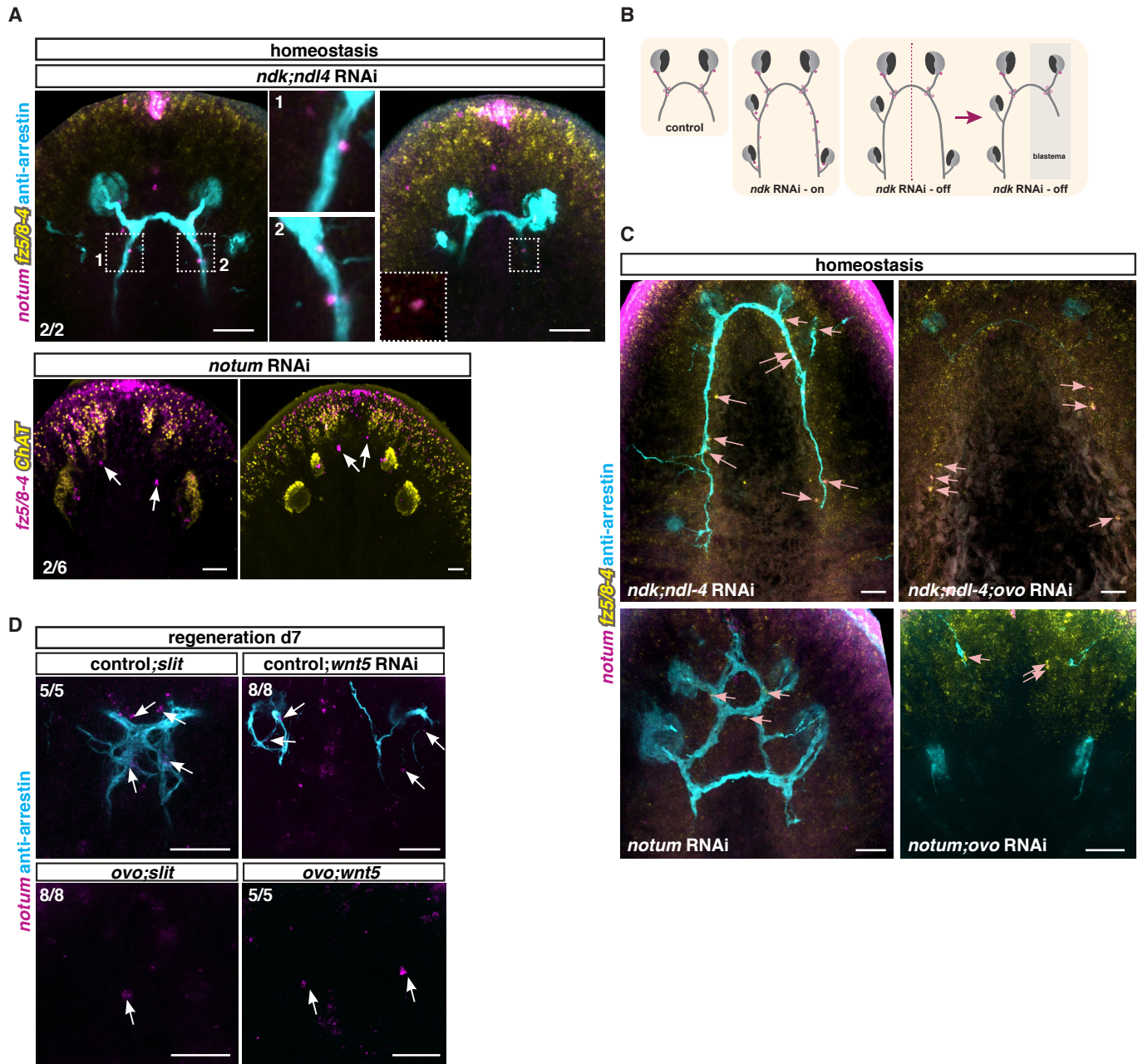


Figure S9

**Figure S9. NME and NMC placement requires positional information.** (A) Ectopic NMEs/NMCs in different uninjured RNAi conditions. NMEs/NMCs can be observed before the nucleation of new ectopic eyes or projection of axons. (B) Illustration summarizing NME/NMC distribution in *ndk* RNAi animals before and after wearing off the RNAi and after sagittal amputation. (C) Presence (control) or absence (*ovo* RNAi) of visual axons and distribution of NMEs/NMCs in intact *ndk*; *ndl-4* and *notum* RNAi animals. (D) Location of NMEs/NMCs changed following *wnt5* and *slit* RNAi independently of eye cells.

Scale bars, 50 $\mu$ m (A, C, D).

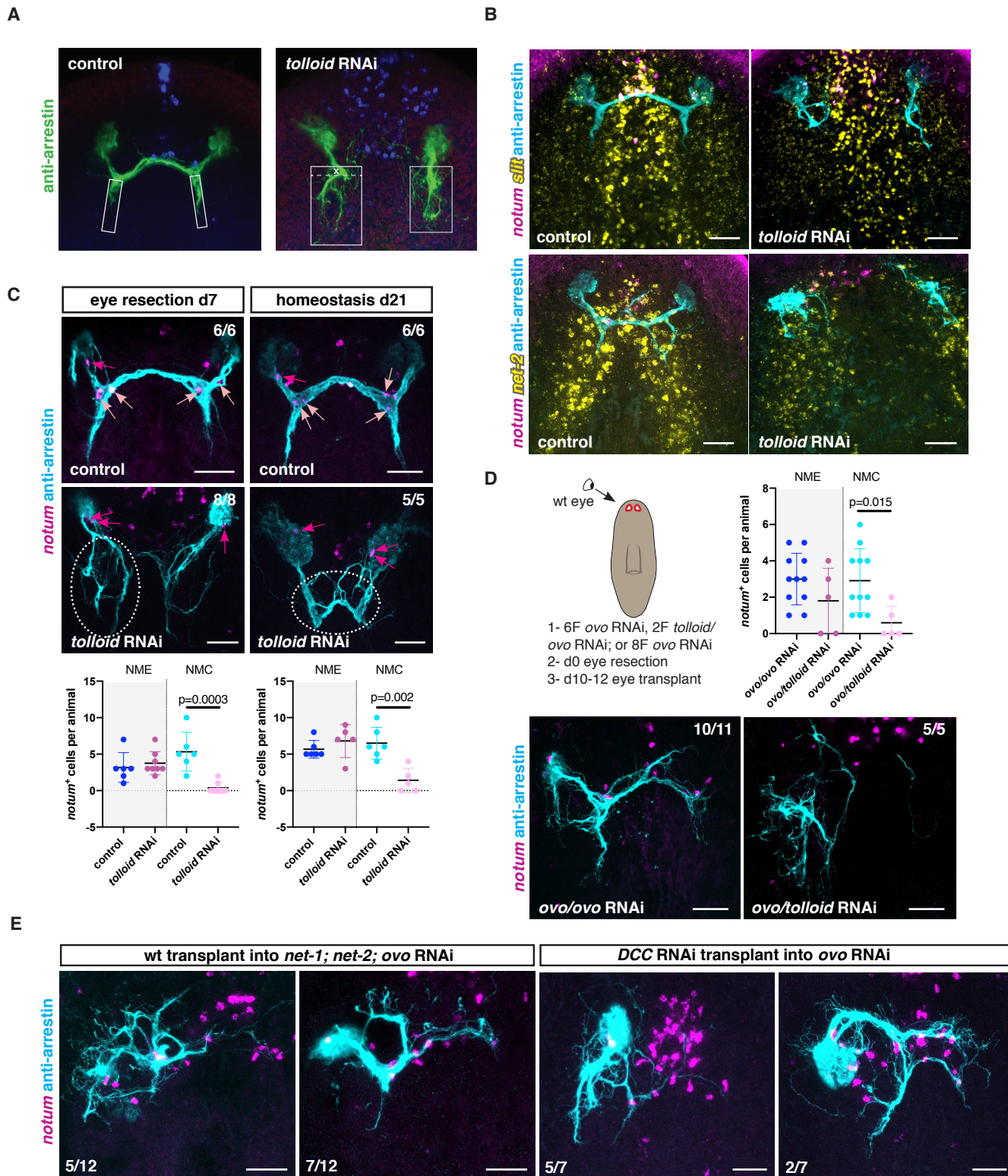


Figure S10

**Figure S10. *tolloid* is required for NMC specification.** (A) Dotted area shows how the width of axonal projections was quantified in Fig. 6. (B) Normal expression of the guidance cues *slit* and *netrin-2* in uninjured *tolloid* RNAi animals. (C) Defasciculation of visual axons (white dotted line) and reduced numbers or complete absence of NMCs in a regenerating double-eye resected *tolloid* RNAi animal, and in an uninjured *tolloid* RNAi animal. Below, graphs show NME/NMC numbers in the different conditions. (D) Top left, cartoon shows summary of eye transplantation protocol. Top right, graph shows NME/NMC numbers after a wildtype eye transplantation in *ovo* or *ovo/tolloid* RNAi recipients. Below: Visual axons of eyes transplanted into *ovo/tolloid* RNAi recipients did not recapitulate the stereotypical route of the visual axonal trajectories. (E) Axons from wildtype eyes transplanted into *netrin-1; netrin-2; ovo* RNAi animals do not project contralaterally. Similarly, axons from *DCC* RNAi eyes transplanted into *ovo* RNAi recipients are aberrant and show disrupted projection patterns.

Scale bars, 50µm (B-E).

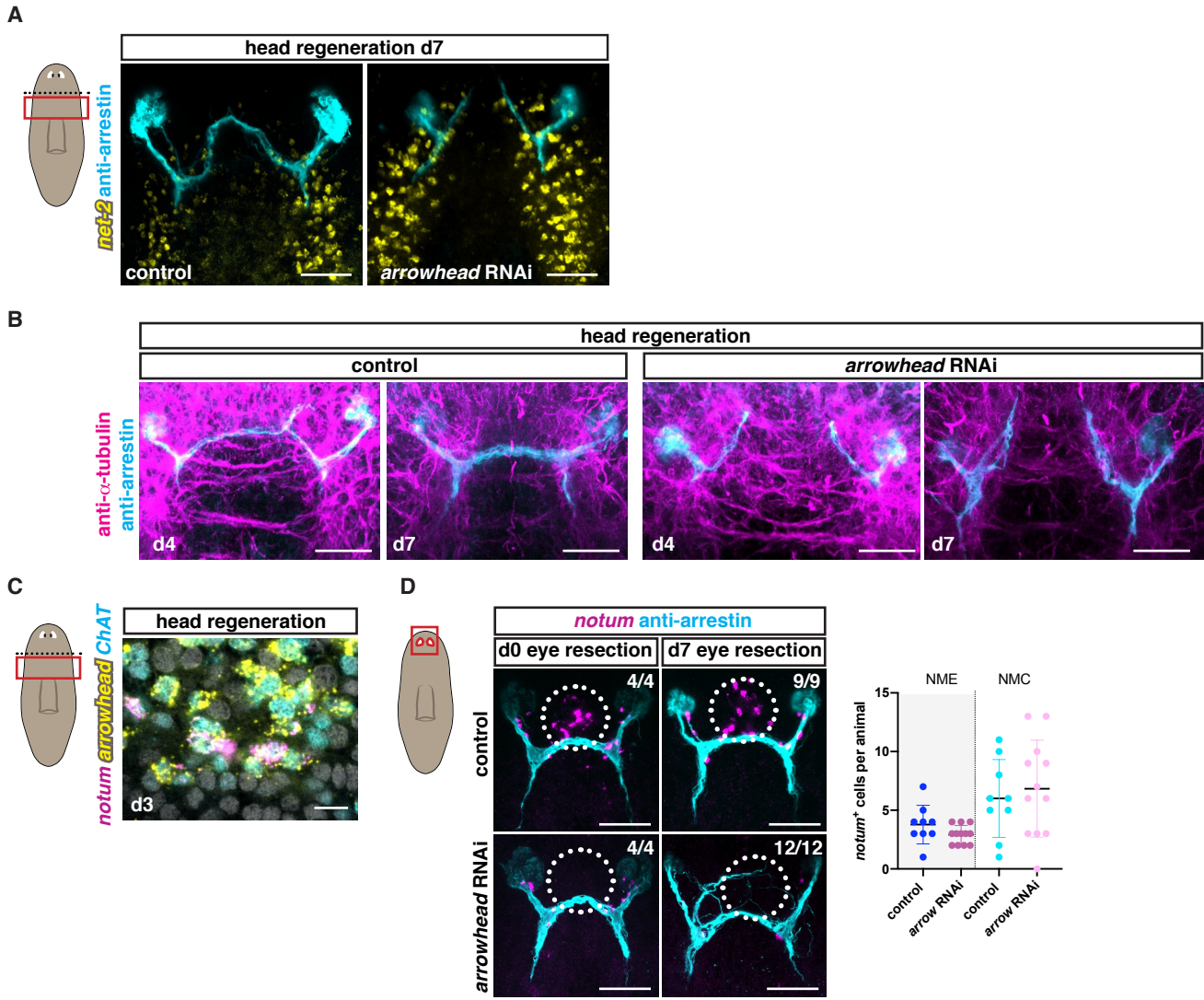


Figure S11

**Figure S11. *arrowhead* is required for NBC specification and optic chiasm regeneration.** (A) Normal expression of the guidance cue *netrin-2* in an *arrowhead* RNAi animal that did not regenerate the optic chiasm after head amputation. (B) Visual axons in regenerating control and *arrowhead* RNAi animals do not obviously follow other axonal bundles at the anterior commissure. (C) NBCs express the transcription factor *arrowhead* in regenerating animals. (D) Normal stereotypical visual axonal trajectories in a double-eye resected *arrowhead* RNAi animal that lacks NBCs (white dotted circles). Right: graph shows normal numbers of NMEs/NMCs in double-eye resected *arrowhead* RNAi animals. Dotted black lines in cartoons show amputation planes, red boxes show location of image taken.

Scale bars, 50 $\mu$ m (A-D).



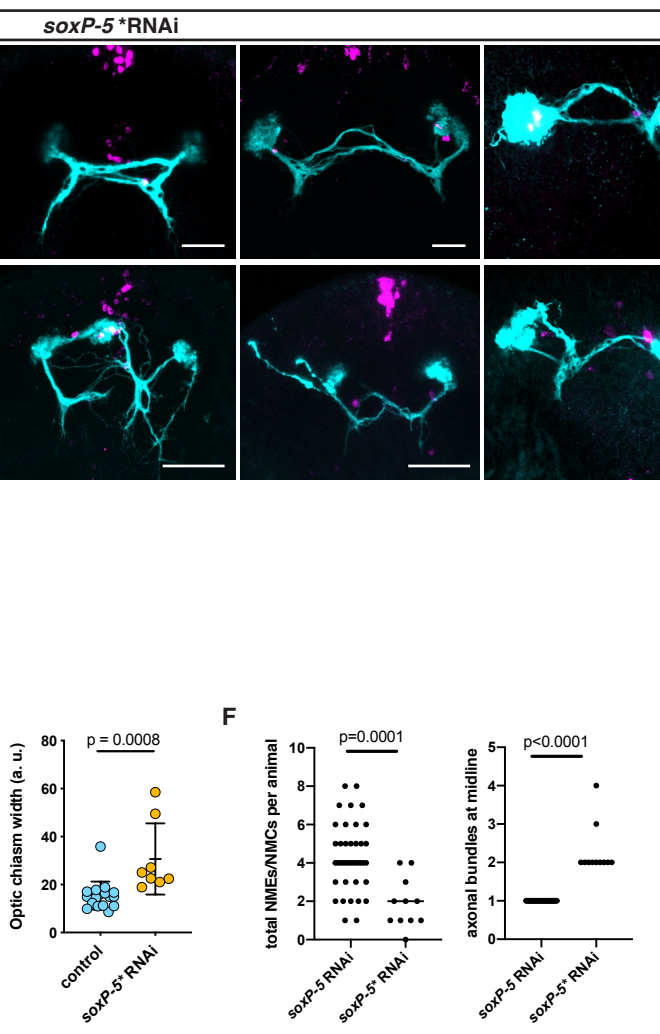
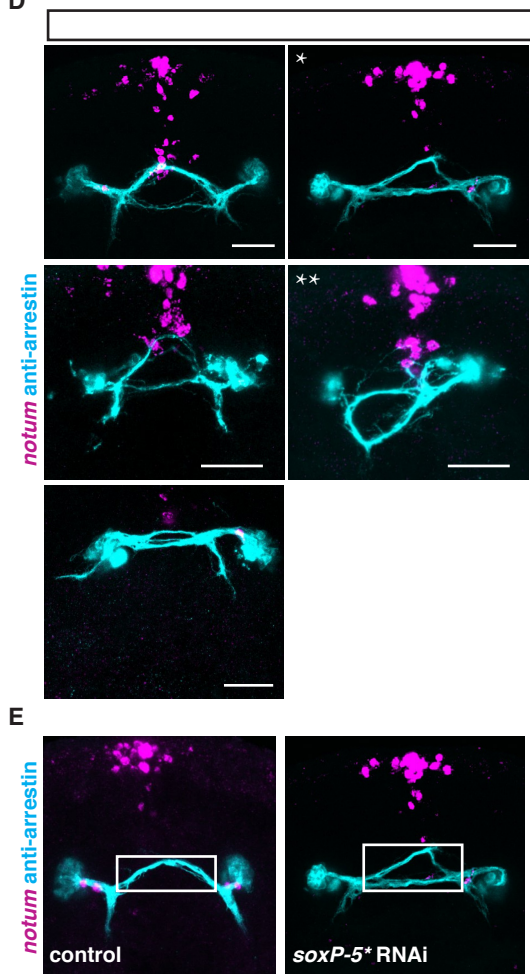
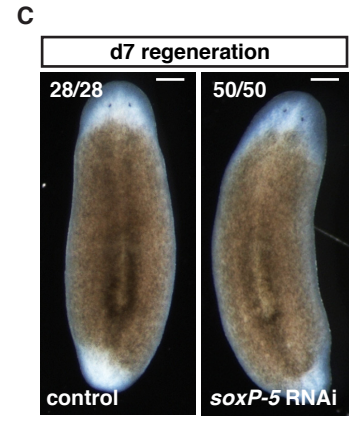
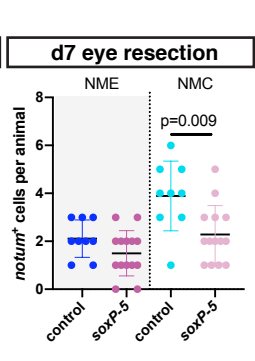
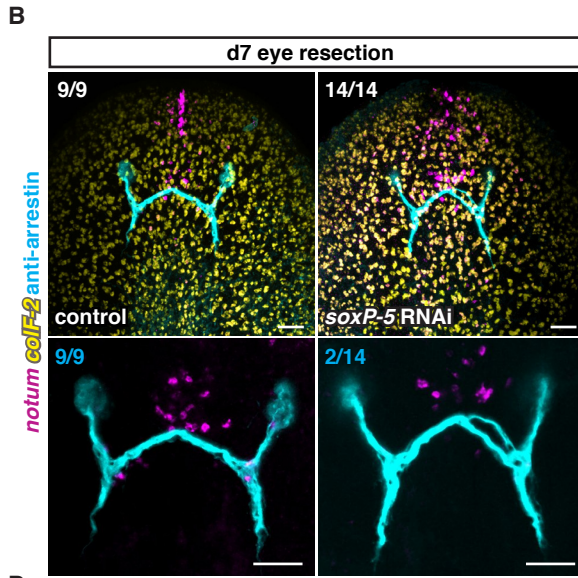
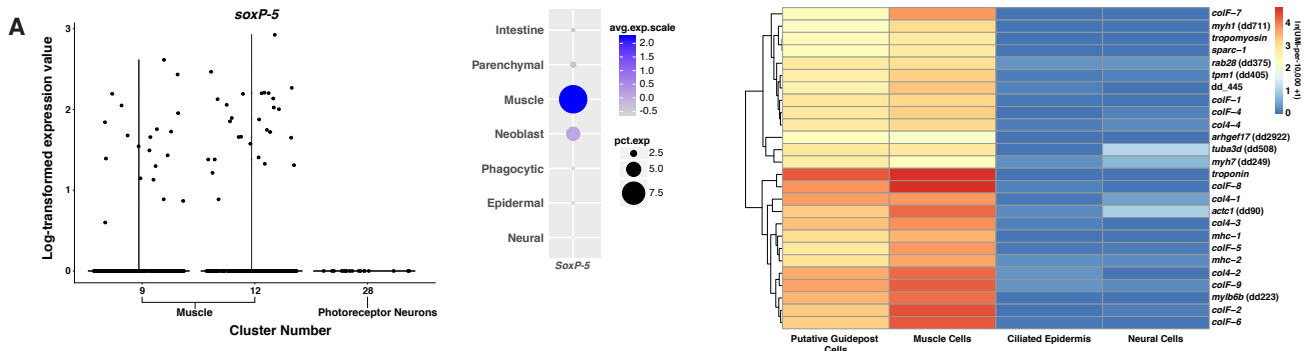
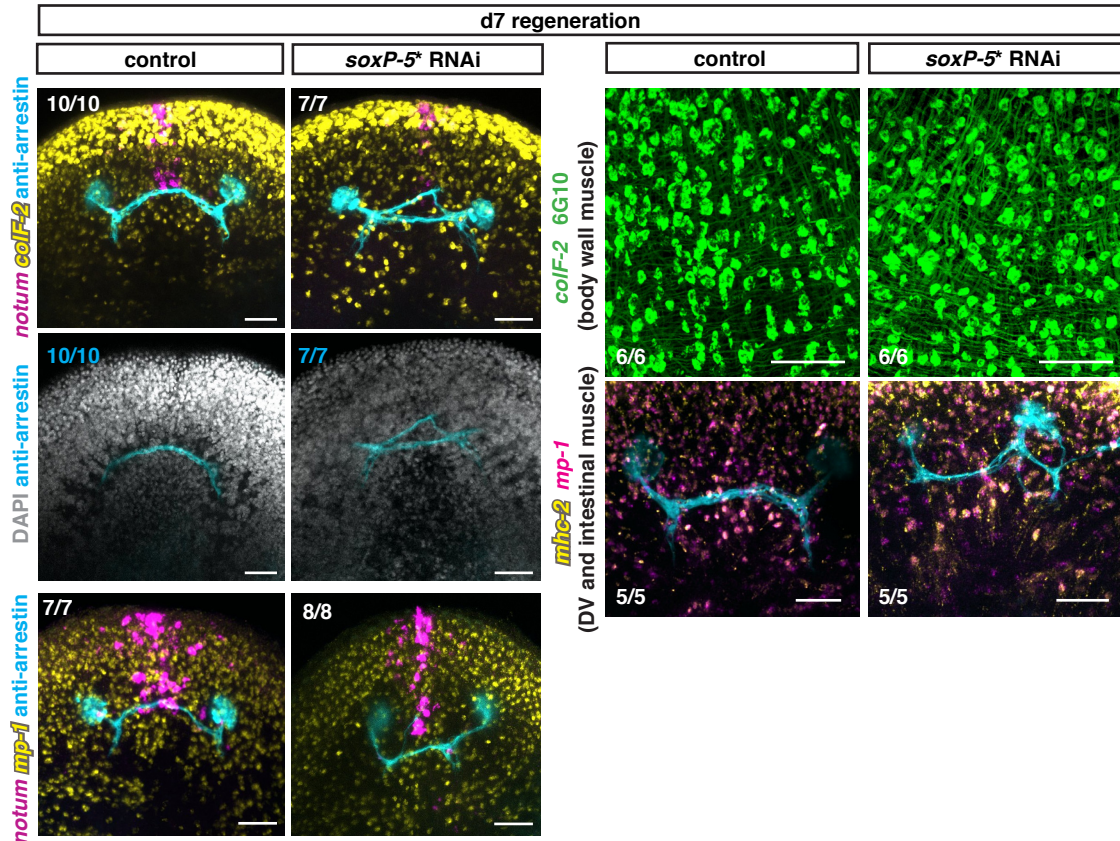


Figure S12

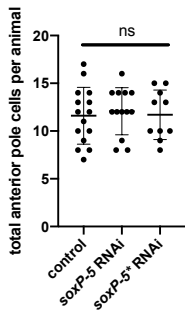
**Figure S12. *soxP-5* is required for NME and NMC specification.** (A) Violin plot and dot plot show expression of *soxP-5* in different cell types (62). Heatmap shows expression of muscle markers in guidepost-like cells, muscle, epidermal or neuronal cells (62). (B) Minor defasciculations following double-eye resections in a *soxP-5* RNAi animal. Normal expression of the muscle marker *colF-2* and anterior pole (*notum*<sup>+</sup>) in a *soxP-5* RNAi animal. Right: Graph shows reduced numbers of NMEs/NMCs in double-eye resected *soxP-5* RNAi animals. (C) Normal blastema formation in a regenerating *soxP-5* RNAi animal. (D) Images of regenerating *soxP-5*<sup>\*</sup> RNAi animals showing defects in visual axonal wiring. <sup>\*</sup>also shown in S12E, <sup>\*\*</sup>also shown in Fig. 6K. (E) White box shows the area width used for quantification of the *soxP-5*<sup>\*</sup> RNAi phenotype shown in graph on the right. (F) Quantification showing reduced number of NMEs/NMCs in *soxP-5*<sup>\*</sup> animals and increased number of aberrant axon bundles.

Scale bars: 50μm (B-D).

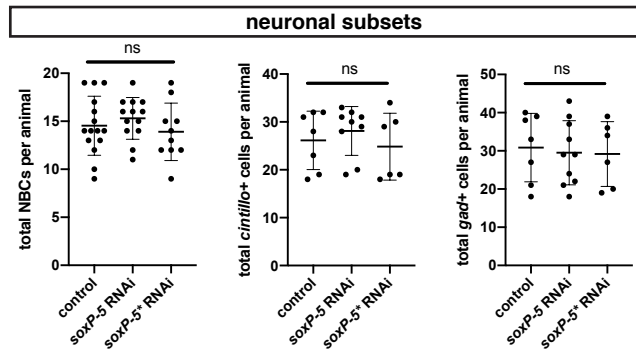
A



B



C



D

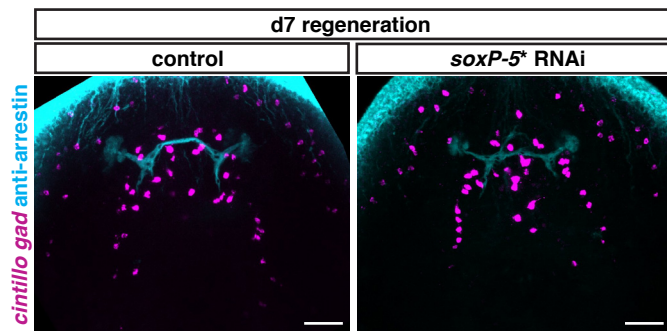


Figure S13

**Figure S13. *soxP-5\** RNAi animals have normal muscle and brain architecture.** (A)

Normal expression of the muscle markers *colF-2*, *mp-1*, *mhc-2*; normal body wall muscle architecture (6G10 ab staining); normal regeneration of anterior pole cells (*notum*<sup>+</sup>); and normal brain architecture (DAPI) in a regenerating *soxP-5\** RNAi animal with an abnormal visual system. (B, C) Quantifications showing that total number of muscle anterior pole cells (B), and neuronal subsets NBCs, *cintillo*<sup>+</sup>, and *gad*<sup>+</sup> cells (C) are unaffected in *soxP-5\** RNAi animals. (D) FISH showing a normal pattern of *cintillo*<sup>+</sup> and *gad*<sup>+</sup> neurons in a regenerating *soxP-5\** RNAi animal.

Scale bars: 50μm (A, D).

## References and Notes

1. J. S. Edwards, S. W. Chen, M. W. Berns, Cercal sensory development following laser microlesions of embryonic apical cells in *Acheta domesticus*. *J. Neurosci.* **1**, 250–258 (1981). [doi:10.1523/JNEUROSCI.01-03-00250.1981](https://doi.org/10.1523/JNEUROSCI.01-03-00250.1981) [Medline](#)
2. H. Hutter, Extracellular cues and pioneers act together to guide axons in the ventral cord of *C. elegans*. *Development* **130**, 5307–5318 (2003). [doi:10.1242/dev.00727](https://doi.org/10.1242/dev.00727) [Medline](#)
3. M. Klose, D. Bentley, Transient pioneer neurons are essential for formation of an embryonic peripheral nerve. *Science* **245**, 982–984 (1989). [doi:10.1126/science.2772651](https://doi.org/10.1126/science.2772651) [Medline](#)
4. S. H. Pike, E. F. Melancon, J. S. Eisen, Pathfinding by zebrafish motoneurons in the absence of normal pioneer axons. *Development* **114**, 825–831 (1992). [Medline](#)
5. A. L. Kolodkin, M. Tessier-Lavigne, Mechanisms and molecules of neuronal wiring: A primer. *Cold Spring Harb. Perspect. Biol.* **3**, a001727 (2011). [doi:10.1101/cshperspect.a001727](https://doi.org/10.1101/cshperspect.a001727) [Medline](#)
6. E. T. Stoeckli, Understanding axon guidance: Are we nearly there yet? *Development* **145**, dev151415 (2018). [doi:10.1242/dev.151415](https://doi.org/10.1242/dev.151415) [Medline](#)
7. M. Tessier-Lavigne, C. S. Goodman, The molecular biology of axon guidance. *Science* **274**, 1123–1133 (1996). [doi:10.1126/science.274.5290.1123](https://doi.org/10.1126/science.274.5290.1123) [Medline](#)
8. T. W. Yu, C. I. Bargmann, Dynamic regulation of axon guidance. *Nat. Neurosci.* **4** (Suppl), 1169–1176 (2001). [doi:10.1038/nn748](https://doi.org/10.1038/nn748) [Medline](#)
9. D. Bentley, M. Caudy, Pioneer axons lose directed growth after selective killing of guidepost cells. *Nature* **304**, 62–65 (1983). [doi:10.1038/304062a0](https://doi.org/10.1038/304062a0) [Medline](#)
10. D. Bentley, H. Keshishian, Pathfinding by peripheral pioneer neurons in grasshoppers. *Science* **218**, 1082–1088 (1982). [doi:10.1126/science.218.4577.1082](https://doi.org/10.1126/science.218.4577.1082) [Medline](#)
11. D. L. Chao, L. Ma, K. Shen, Transient cell-cell interactions in neural circuit formation. *Nat. Rev. Neurosci.* **10**, 262–271 (2009). [doi:10.1038/nrn2594](https://doi.org/10.1038/nrn2594) [Medline](#)
12. P. Squarzoni, M. S. Thion, S. Garel, Neuronal and microglial regulators of cortical wiring: Usual and novel guideposts. *Front. Neurosci.* **9**, 248 (2015). [doi:10.3389/fnins.2015.00248](https://doi.org/10.3389/fnins.2015.00248) [Medline](#)
13. T. Hirata, T. Kumada, T. Kawasaki, T. Furukawa, A. Aiba, F. Conquet, Y. Saga, A. Fukuda, Guidepost neurons for the lateral olfactory tract: Expression of metabotropic glutamate receptor 1 and innervation by glutamatergic olfactory bulb axons. *Dev. Neurobiol.* **72**, 1559–1576 (2012). [doi:10.1002/dneu.22030](https://doi.org/10.1002/dneu.22030) [Medline](#)
14. G. López-Bendito, A. Cautinat, J. A. Sánchez, F. Bielle, N. Flames, A. N. Garratt, D. A. Talmage, L. W. Role, P. Charnay, O. Marín, S. Garel, Tangential neuronal migration controls axon guidance: A role for neuregulin-1 in thalamocortical axon navigation. *Cell* **125**, 127–142 (2006). [doi:10.1016/j.cell.2006.01.042](https://doi.org/10.1016/j.cell.2006.01.042) [Medline](#)
15. M. Niquille, S. Garel, F. Mann, J.-P. Hornung, B. Otsmane, S. Chevalley, C. Parras, F. Guillemot, P. Gaspar, Y. Yanagawa, C. Lebrand, Transient neuronal populations are required to guide callosal axons: A role for semaphorin 3C. *PLOS Biol.* **7**, e1000230 (2009). [doi:10.1371/journal.pbio.1000230](https://doi.org/10.1371/journal.pbio.1000230) [Medline](#)

16. Y. Sato, T. Hirata, M. Ogawa, H. Fujisawa, Requirement for early-generated neurons recognized by monoclonal antibody lot1 in the formation of lateral olfactory tract. *J. Neurosci.* **18**, 7800–7810 (1998). [doi:10.1523/JNEUROSCI.18-19-07800.1998](https://doi.org/10.1523/JNEUROSCI.18-19-07800.1998) [Medline](#)
17. F. Bielle, P. Marcos-Mondejar, M. Keita, C. Mailhes, C. Verney, K. Nguyen Ba-Charvet, M. Tessier-Lavigne, G. Lopez-Bendito, S. Garel, Slit2 activity in the migration of guidepost neurons shapes thalamic projections during development and evolution. *Neuron* **69**, 1085–1098 (2011). [doi:10.1016/j.neuron.2011.02.026](https://doi.org/10.1016/j.neuron.2011.02.026) [Medline](#)
18. K. Ito, T. Kawasaki, S. Takashima, I. Matsuda, A. Aiba, T. Hirata, Semaphorin 3F confines ventral tangential migration of lateral olfactory tract neurons onto the telencephalon surface. *J. Neurosci.* **28**, 4414–4422 (2008). [doi:10.1523/JNEUROSCI.0372-08.2008](https://doi.org/10.1523/JNEUROSCI.0372-08.2008) [Medline](#)
19. T. Kawasaki, K. Ito, T. Hirata, Netrin 1 regulates ventral tangential migration of guidepost neurons in the lateral olfactory tract. *Development* **133**, 845–853 (2006). [doi:10.1242/dev.02257](https://doi.org/10.1242/dev.02257) [Medline](#)
20. T. Nomura, J. Holmberg, J. Frisen, N. Osumi, Pax6-dependent boundary defines alignment of migrating olfactory cortex neurons via the repulsive activity of ephrin A5. *Development* **133**, 1335–1345 (2006). [doi:10.1242/dev.02290](https://doi.org/10.1242/dev.02290) [Medline](#)
21. R. R. Bernhardt, C. K. Patel, S. W. Wilson, J. Y. Kuwada, Axonal trajectories and distribution of GABAergic spinal neurons in wildtype and mutant zebrafish lacking floor plate cells. *J. Comp. Neurol.* **326**, 263–272 (1992). [doi:10.1002/cne.903260208](https://doi.org/10.1002/cne.903260208) [Medline](#)
22. C. Klämbt, J. R. Jacobs, C. S. Goodman, The midline of the Drosophila central nervous system: A model for the genetic analysis of cell fate, cell migration, and growth cone guidance. *Cell* **64**, 801–815 (1991). [doi:10.1016/0092-8674\(91\)90509-W](https://doi.org/10.1016/0092-8674(91)90509-W) [Medline](#)
23. R. C. Marcus, R. Blazeski, P. Godement, C. A. Mason, Retinal axon divergence in the optic chiasm: Uncrossed axons diverge from crossed axons within a midline glial specialization. *J. Neurosci.* **15**, 3716–3729 (1995). [doi:10.1523/JNEUROSCI.15-05-03716.1995](https://doi.org/10.1523/JNEUROSCI.15-05-03716.1995) [Medline](#)
24. D. W. Sretavan, L. Feng, E. Puré, L. F. Reichardt, Embryonic neurons of the developing optic chiasm express L1 and CD44, cell surface molecules with opposing effects on retinal axon growth. *Neuron* **12**, 957–975 (1994). [doi:10.1016/0896-6273\(94\)90307-7](https://doi.org/10.1016/0896-6273(94)90307-7) [Medline](#)
25. R. Amamoto, V. G. L. Huerta, E. Takahashi, G. Dai, A. K. Grant, Z. Fu, P. Arlotta, Adult axolotls can regenerate original neuronal diversity in response to brain injury. *eLife* **5**, e13998 (2016). [doi:10.7554/eLife.13998](https://doi.org/10.7554/eLife.13998) [Medline](#)
26. C. E. Laumer, N. Bekkouche, A. Kerbl, F. Goetz, R. C. Neves, M. V. Sørensen, R. M. Kristensen, A. Hejnol, C. W. Dunn, G. Giribet, K. Worsaae, Spiralian phylogeny informs the evolution of microscopic lineages. *Curr. Biol.* **25**, 2000–2006 (2015). [doi:10.1016/j.cub.2015.06.068](https://doi.org/10.1016/j.cub.2015.06.068) [Medline](#)
27. J. N. Witchley, M. Mayer, D. E. Wagner, J. H. Owen, P. W. Reddien, Muscle cells provide instructions for planarian regeneration. *Cell Rep.* **4**, 633–641 (2013). [doi:10.1016/j.celrep.2013.07.022](https://doi.org/10.1016/j.celrep.2013.07.022) [Medline](#)

28. K. Agata, Y. Soejima, K. Kato, C. Kobayashi, Y. Umesono, K. Watanabe, Structure of the planarian central nervous system (CNS) revealed by neuronal cell markers. *Zool. Sci.* **15**, 433–440 (1998). [doi:10.2108/zsj.15.433](https://doi.org/10.2108/zsj.15.433) [Medline](#)
29. K. Okamoto, K. Takeuchi, K. Agata, Neural projections in planarian brain revealed by fluorescent dye tracing. *Zool. Sci.* **22**, 535–546 (2005). [doi:10.2108/zsj.22.535](https://doi.org/10.2108/zsj.22.535) [Medline](#)
30. F. Sakai, K. Agata, H. Orii, K. Watanabe, Organization and regeneration ability of spontaneous supernumerary eyes in planarians—eye regeneration field and pathway selection by optic nerves—. *Zool. Sci.* **17**, 375–381 (2000). [Medline](#)
31. C. P. Petersen, P. W. Reddien, Polarized *notum* activation at wounds inhibits Wnt function to promote planarian head regeneration. *Science* **332**, 852–855 (2011). [doi:10.1126/science.1202143](https://doi.org/10.1126/science.1202143) [Medline](#)
32. E. M. Hill, C. P. Petersen, Wnt/Notum spatial feedback inhibition controls neoblast differentiation to regulate reversible growth of the planarian brain. *Development* **142**, 4217–4229 (2015). [doi:10.1242/dev.123612](https://doi.org/10.1242/dev.123612) [Medline](#)
33. P. W. Reddien, The cellular and molecular basis for planarian regeneration. *Cell* **175**, 327–345 (2018). [doi:10.1016/j.cell.2018.09.021](https://doi.org/10.1016/j.cell.2018.09.021) [Medline](#)
34. S. W. Lapan, P. W. Reddien, *dlx* and *sp6-9* control optic cup regeneration in a prototypic eye. *PLOS Genet.* **7**, e1002226 (2011). [doi:10.1371/journal.pgen.1002226](https://doi.org/10.1371/journal.pgen.1002226) [Medline](#)
35. M. L. Scimone, M. Srivastava, G. W. Bell, P. W. Reddien, A regulatory program for excretory system regeneration in planarians. *Development* **138**, 4387–4398 (2011). [doi:10.1242/dev.068098](https://doi.org/10.1242/dev.068098) [Medline](#)
36. M. L. Scimone, L. E. Cote, P. W. Reddien, Orthogonal muscle fibres have different instructive roles in planarian regeneration. *Nature* **551**, 623–628 (2017). [doi:10.1038/nature24660](https://doi.org/10.1038/nature24660) [Medline](#)
37. M. L. Scimone, O. Wurtzel, K. Malecek, C. T. Fincher, I. M. Oderberg, K. M. Kravarik, P. W. Reddien, *foxF-1* controls specification of non-body wall muscle and phagocytic cells in planarians. *Curr. Biol.* **28**, 3787–3801.e6 (2018). [doi:10.1016/j.cub.2018.10.030](https://doi.org/10.1016/j.cub.2018.10.030) [Medline](#)
38. S. A. LoCascio, S. W. Lapan, P. W. Reddien, Eye absence does not regulate planarian stem cells during eye regeneration. *Dev. Cell* **40**, 381–391.e3 (2017). [doi:10.1016/j.devcel.2017.02.002](https://doi.org/10.1016/j.devcel.2017.02.002) [Medline](#)
39. T. J. Petros, A. Rebsam, C. A. Mason, Retinal axon growth at the optic chiasm: To cross or not to cross. *Annu. Rev. Neurosci.* **31**, 295–315 (2008). [doi:10.1146/annurev.neuro.31.060407.125609](https://doi.org/10.1146/annurev.neuro.31.060407.125609) [Medline](#)
40. T. Inoue, H. Kumamoto, K. Okamoto, Y. Umesono, M. Sakai, A. Sánchez Alvarado, K. Agata, Morphological and functional recovery of the planarian photosensing system during head regeneration. *Zool. Sci.* **21**, 275–283 (2004). [doi:10.2108/zsj.21.275](https://doi.org/10.2108/zsj.21.275) [Medline](#)
41. K. D. Atabay, S. A. LoCascio, T. de Hoog, P. W. Reddien, Self-organization and progenitor targeting generate stable patterns in planarian regeneration. *Science* **360**, 404–409 (2018). [doi:10.1126/science.aap8179](https://doi.org/10.1126/science.aap8179) [Medline](#)

42. S. W. Lapan, P. W. Reddien, Transcriptome analysis of the planarian eye identifies *ovo* as a specific regulator of eye regeneration. *Cell Rep.* **2**, 294–307 (2012). [doi:10.1016/j.celrep.2012.06.018](https://doi.org/10.1016/j.celrep.2012.06.018) [Medline](#)
43. F. Cebrià, P. A. Newmark, Planarian homologs of *netrin* and *netrin receptor* are required for proper regeneration of the central nervous system and the maintenance of nervous system architecture. *Development* **132**, 3691–3703 (2005). [doi:10.1242/dev.01941](https://doi.org/10.1242/dev.01941) [Medline](#)
44. P. A. Newmark, P. W. Reddien, F. Cebrià, A. Sánchez Alvarado, Ingestion of bacterially expressed double-stranded RNA inhibits gene expression in planarians. *Proc. Natl. Acad. Sci. U.S.A.* **100** (suppl 1.), 11861–11865 (2003). [doi:10.1073/pnas.1834205100](https://doi.org/10.1073/pnas.1834205100) [Medline](#)
45. F. Cebrià, T. Guo, J. Jopek, P. A. Newmark, Regeneration and maintenance of the planarian midline is regulated by a *slit* orthologue. *Dev. Biol.* **307**, 394–406 (2007). [doi:10.1016/j.ydbio.2007.05.006](https://doi.org/10.1016/j.ydbio.2007.05.006) [Medline](#)
46. F. Cebrià, P. A. Newmark, Morphogenesis defects are associated with abnormal nervous system regeneration following *roboA* RNAi in planarians. *Development* **134**, 833–837 (2007). [doi:10.1242/dev.02794](https://doi.org/10.1242/dev.02794) [Medline](#)
47. M. L. Scimone, L. E. Cote, T. Rogers, P. W. Reddien, Two FGFR1-Wnt circuits organize the planarian anteroposterior axis. *eLife* **5**, e12845 (2016). [doi:10.7554/eLife.12845](https://doi.org/10.7554/eLife.12845) [Medline](#)
48. F. Cebrià, C. Kobayashi, Y. Umesono, M. Nakazawa, K. Mineta, K. Ikeo, T. Gojobori, M. Itoh, M. Taira, A. Sánchez Alvarado, K. Agata, FGFR-related gene *nou-darake* restricts brain tissues to the head region of planarians. *Nature* **419**, 620–624 (2002). [doi:10.1038/nature01042](https://doi.org/10.1038/nature01042) [Medline](#)
49. R. Lander, C. P. Petersen, Wnt, Ptk7, and FGFR1 expression gradients control trunk positional identity in planarian regeneration. *eLife* **5**, e12850 (2016). [doi:10.7554/eLife.12850](https://doi.org/10.7554/eLife.12850) [Medline](#)
50. K. A. Gurley, S. A. Elliott, O. Simakov, H. A. Schmidt, T. W. Holstein, A. Sánchez Alvarado, Expression of secreted Wnt pathway components reveals unexpected complexity of the planarian amputation response. *Dev. Biol.* **347**, 24–39 (2010). [doi:10.1016/j.ydbio.2010.08.007](https://doi.org/10.1016/j.ydbio.2010.08.007) [Medline](#)
51. A. Augsburger, A. Schuchardt, S. Hoskins, J. Dodd, S. Butler, BMPs as mediators of roof plate repulsion of commissural neurons. *Neuron* **24**, 127–141 (1999). [doi:10.1016/S0896-6273\(00\)80827-2](https://doi.org/10.1016/S0896-6273(00)80827-2) [Medline](#)
52. S. J. Butler, J. Dodd, A role for BMP heterodimers in roof plate-mediated repulsion of commissural axons. *Neuron* **38**, 389–401 (2003). [doi:10.1016/S0896-6273\(03\)00254-X](https://doi.org/10.1016/S0896-6273(03)00254-X) [Medline](#)
53. P. W. Reddien, A. L. Bermange, A. M. Kicza, A. Sánchez Alvarado, BMP signaling regulates the dorsal planarian midline and is needed for asymmetric regeneration. *Development* **134**, 4043–4051 (2007). [doi:10.1242/dev.007138](https://doi.org/10.1242/dev.007138) [Medline](#)
54. P. Blader, S. Rastegar, N. Fischer, U. Strähle, Cleavage of the BMP-4 antagonist chordin by zebrafish Tolloid. *Science* **278**, 1937–1940 (1997). [doi:10.1126/science.278.5345.1937](https://doi.org/10.1126/science.278.5345.1937) [Medline](#)



55. S. Piccolo, E. Agius, B. Lu, S. Goodman, L. Dale, E. M. De Robertis, Cleavage of Chordin by Xolloid metalloprotease suggests a role for proteolytic processing in the regulation of Spemann organizer activity. *Cell* **91**, 407–416 (1997). [doi:10.1016/S0092-8674\(00\)80424-9](https://doi.org/10.1016/S0092-8674(00)80424-9) [Medline](#)
56. M. J. Galko, M. Tessier-Lavigne, Function of an axonal chemoattractant modulated by metalloprotease activity. *Science* **289**, 1365–1367 (2000). [doi:10.1126/science.289.5483.1365](https://doi.org/10.1126/science.289.5483.1365) [Medline](#)
57. D. W. Sretavan, E. Puré, M. W. Siegel, L. F. Reichardt, Disruption of retinal axon ingrowth by ablation of embryonic mouse optic chiasm neurons. *Science* **269**, 98–101 (1995). [doi:10.1126/science.7541558](https://doi.org/10.1126/science.7541558) [Medline](#)
58. M. W. Cowles, D. D. R. Brown, S. V. Nisperos, B. N. Stanley, B. J. Pearson, R. M. Zayas, Genome-wide analysis of the bHLH gene family in planarians identifies factors required for adult neurogenesis and neuronal regeneration. *Development* **140**, 4691–4702 (2013). [doi:10.1242/dev.098616](https://doi.org/10.1242/dev.098616) [Medline](#)
59. M. L. Scimone, K. M. Kravarik, S. W. Lapan, P. W. Reddien, Neoblast specialization in regeneration of the planarian *Schmidtea mediterranea*. *Stem Cell Reports* **3**, 339–352 (2014). [doi:10.1016/j.stemcr.2014.06.001](https://doi.org/10.1016/j.stemcr.2014.06.001) [Medline](#)
60. R. H. Roberts-Galbraith, J. L. Brubacher, P. A. Newmark, A functional genomics screen in planarians reveals regulators of whole-brain regeneration. *eLife* **5**, e17002 (2016). [doi:10.7554/eLife.17002](https://doi.org/10.7554/eLife.17002) [Medline](#)
61. E. Z. Macosko, A. Basu, R. Satija, J. Nemes, K. Shekhar, M. Goldman, I. Tirosh, A. R. Bialas, N. Kamitaki, E. M. Martersteck, J. J. Trombetta, D. A. Weitz, J. R. Sanes, A. K. Shalek, A. Regev, S. A. McCarroll, Highly parallel genome-wide expression profiling of individual cells using nanoliter droplets. *Cell* **161**, 1202–1214 (2015). [doi:10.1016/j.cell.2015.05.002](https://doi.org/10.1016/j.cell.2015.05.002) [Medline](#)
62. C. T. Fincher, O. Wurtzel, T. de Hoog, K. M. Kravarik, P. W. Reddien, Cell type transcriptome atlas for the planarian *Schmidtea mediterranea*. *Science* **360**, eaaq1736 (2018). [doi:10.1126/science.aaq1736](https://doi.org/10.1126/science.aaq1736) [Medline](#)
63. L. E. Cote, E. Simental, P. W. Reddien, Muscle functions as a connective tissue and source of extracellular matrix in planarians. *Nat. Commun.* **10**, 1592 (2019). [doi:10.1038/s41467-019-09539-6](https://doi.org/10.1038/s41467-019-09539-6) [Medline](#)
64. I. M. Oderberg, D. J. Li, M. L. Scimone, M. A. Gaviño, P. W. Reddien, Landmarks in existing tissue at wounds are utilized to generate pattern in regenerating tissue. *Curr. Biol.* **27**, 733–742 (2017). [doi:10.1016/j.cub.2017.01.024](https://doi.org/10.1016/j.cub.2017.01.024) [Medline](#)
65. T. Hayashi, M. Motoishi, S. Yazawa, K. Itomi, C. Tanegashima, O. Nishimura, K. Agata, H. Tarui, A LIM-homeobox gene is required for differentiation of Wnt-expressing cells at the posterior end of the planarian body. *Development* **138**, 3679–3688 (2011). [doi:10.1242/dev.060194](https://doi.org/10.1242/dev.060194) [Medline](#)
66. C. P. Petersen, P. W. Reddien, Wnt signaling and the polarity of the primary body axis. *Cell* **139**, 1056–1068 (2009). [doi:10.1016/j.cell.2009.11.035](https://doi.org/10.1016/j.cell.2009.11.035) [Medline](#)

67. A. Jaworski, M. Tessier-Lavigne, Autocrine/juxtacrine regulation of axon fasciculation by Slit-Robo signaling. *Nat. Neurosci.* **15**, 367–369 (2012). [doi:10.1038/nn.3037](https://doi.org/10.1038/nn.3037) [Medline](#)
68. J. M. Martín-Durán, E. Amaya, R. Romero, Germ layer specification and axial patterning in the embryonic development of the freshwater planarian *Schmidtea polychroa*. *Dev. Biol.* **340**, 145–158 (2010). [doi:10.1016/j.ydbio.2010.01.018](https://doi.org/10.1016/j.ydbio.2010.01.018) [Medline](#)
69. R. Satija, J. A. Farrell, D. Gennert, A. F. Schier, A. Regev, Spatial reconstruction of single-cell gene expression data. *Nat. Biotechnol.* **33**, 495–502 (2015). [doi:10.1038/nbt.3192](https://doi.org/10.1038/nbt.3192) [Medline](#)
70. P. V. Kharchenko, L. Silberstein, D. T. Scadden, Bayesian approach to single-cell differential expression analysis. *Nat. Methods* **11**, 740–742 (2014). [doi:10.1038/nmeth.2967](https://doi.org/10.1038/nmeth.2967) [Medline](#)
71. K. G. Ross, K. C. Omuro, M. R. Taylor, R. K. Munday, A. Hubert, R. S. King, R. M. Zayas, Novel monoclonal antibodies to study tissue regeneration in planarians. *BMC Dev. Biol.* **15**, 2 (2015). [doi:10.1186/s12861-014-0050-9](https://doi.org/10.1186/s12861-014-0050-9) [Medline](#)